HHS Public Access

Author manuscript

J Pathol. Author manuscript; available in PMC 2016 June 01.

Published in final edited form as:

J Pathol. 2015 June ; 236(2): 241–250. doi:10.1002/path.4511.

X-linked spinal muscular atrophy in mice caused by autonomous loss of ATP7A in the motor neuron

Victoria L. Hodgkinson[1,4,7], **Jeffery M. Dale**[2,4], **Michael L. Garcia**[2,4], **Gary A. Weisman**[1,4], **Jaekwon Lee**[5], **Jonathan D. Gitlin**[6], and **Michael J. Petris**[1,3,4]

[1]Department of Biochemistry, University of Missouri, Columbia, MO, 65211

[2]Department of Biological Sciences, University of Missouri, Columbia, MO, 65211

[3]Department of Nutrition and Exercise Physiology, University of Missouri, Columbia, MO, 65211

[4]Christopher S. Bond Life Science Center, University of Missouri, Columbia, MO, 65211

[5]Redox Biology Center, University of Nebraska, Lincoln, NE, 68588

[6]Marine Biological Laboratory, Woods Hole, MA, 02543

Abstract

ATP7A is a copper transporting P-type ATPase that is essential for cellular copper homeostasis. Loss-of-function mutations in the *ATP7A* gene result in Menkes disease, a fatal neurodegenerative disorder resulting in seizures, hypotonia, and failure to thrive due to systemic copper deficiency. Most recently, rare missense mutations in *ATP7A* that do not impact systemic copper homeostasis have been shown to cause X-linked Spinal Muscular Atrophy type 3 (SMAX3), a distal hereditary motor neuropathy. An understanding of the mechanistic and pathophysiological basis of SMAX3 is currently lacking, in part because the disease-causing mutations have been shown to confer both loss- and gain-of-function properties to ATP7A, and because there is currently no animal model of the disease. In this study, the *Atp7a* gene was specifically deleted in the motor neurons of mice resulting in a degenerative phenotype consistent with the clinical features in affected patients with SMAX3, including the progressive deterioration of gait, age-dependent muscle atrophy, denervation of neuromuscular junctions, and a loss of motor neuron cell bodies. Taken together these data reveal autonomous requirements for ATP7A that reveal essential roles for copper in the maintenance and function of the motor neuron, and suggest that SMAX3 is caused by a loss of ATP7A function that specifically impacts in the spinal motor neuron.

Address correspondence to: Michael Petris, Ph.D. 540d Life Sciences Center, 1201 Rollins St., University of Missouri, Columbia, MO 65211. Ph: +1-573-882-9685. Fax: +1-573-884-2537. petrism@missouri.edu.

[7]Current address: Department of Physiology and Pharmacology, Hotchkiss Brain Institute, University of Calgary, Calgary, AB, Canada, T2N 4N1.

Conflicts of Interest: The authors declare no conflicts of interest

AUTHOR CONTRIBUTIONS

VLH, JMD, JL and MJP performed experiments; VLH, MJP, GAW, MJG and JDG designed the experiments and interpreted results; VLH, MJP and JDG wrote the manuscript.

Supporting information: X-linked spinal muscular atrophy caused by autonomous loss of ATP7A in the motor neuron

Keywords

Motor neuron; Copper; Menkes disease; ATP7A; motor neuropathy; X-linked spinal muscular atrophy

Introduction

ATP7A is a copper transporting P-type ATPase that plays a critical role in cellular copper homeostasis. This protein is localized within membranes of the late secretory pathway of multiple cell types where it functions to provide copper to specific proteins in this compartment and to export copper across the plasma membrane, a process that is dependent upon ATP7A trafficking [1]. Loss-of-function mutations in *ATP7A* result in Menkes disease and a milder allelic variant, Occipital Horn Syndrome. The symptoms of these disorders result from decreased activity of specific copper-dependent enzymes, due to systemic copper deficiency that arises from impaired copper export from the intestinal enterocytes into the plasma [2, 3]. Recently, two unique missense mutations in the *ATP7A* gene, P1386S and T994I, were reported in males from unrelated families with the distal hereditary motor neuropathy, X-linked distal spinal muscular atrophy type 3 (SMAX3; OMIM 300489) [4]. Affected individuals presented with foot deformity (pes cavus) and gait instability, which progressed to distal lower limb weakness and atrophy. The absence of overt signs and symptoms of systemic copper deficiency in these patients [4], suggests that the mechanisms underlying SMAX3 are distinct from those of Menkes disease.

Complementation studies using a yeast mutant lacking the *ATP7A* orthologue, *ccc2*, reveal that the P1386S and T994I mutations reduce copper transport by approximately 20%. [4]. While these findings suggest a model in which SMAX3 is caused by a loss of ATP7A function, still other studies suggest that these mutations cause motor neuropathy through a gain of function mechanism [5]. Both mutations result in a partial mislocalization of ATP7A to the plasma membrane in a transfected motor neuron cell line, and in the case of T994I, this is associated with an abnormal interaction with p97/VCP, an intracellular protein mutated in certain motor neuron diseases [5]. To distinguish between these gain-of-function and loss-of-function models for SMAX3, we generated $Atp7a^{MN/Y}$ mice in which the *Atp7a* gene was specifically deleted within the motor neuron, thus producing a true loss of function allele within this cell type. Affected mice exhibited a degenerative motor neuropathy consisting of the progressive onset of gait defects, muscle atrophy, denervation of neuromuscular junctions and a loss of motor neuron cell bodies. These findings reveal autonomous requirements for ATP7A and copper homeostasis in the function and survival of the motor neuron, and support a model in which SMAX3 is caused by loss of ATP7A function that specifically impacts this cell type.

Materials and Methods

Animals

All animal procedures were reviewed and approved by the Institutional Animal Care and Usage Committee of the University of Missouri. All mice were on the C57BL6 strain

background. Mice were housed in vented cages with 12 hour light-dark cycle and food and water was provided *ad libitum*. A standard Picolab diet 5058 (17 ppm Cu) was used in this study (PMI International, St. Louis, MO, USA). All behavioral tests were performed after 1 p.m. during the light phase of the light/dark cycle in a semi-blinded fashion, with the observer blind to genotype.

Generation of the *Atp7a*$^{MN/Y}$ mice

Floxed mice were generated as previously described [6, 7]. *Atp7a*$^{MN/Y}$ mice were generated by crossing Atp7A$^{fl/+}$ and Atp7A$^{fl/fl}$ females with Mnx1$^{tm4(cre)Tmj}$/J mice (Jackson Laboratory). Atp7A$^{fl/+}$ littermates lacking Cre were used as WT controls. Tail biopsies from offspring were genotyped using PCR primers P1 (5'-GACAATACTACACTGACCATATTCA-3') and P2 (5'-GTTCCACAGAAACTATATGCCTGGG-3'). Detection of the Cre transgene was achieved using primers CreF (5'- GATCGCTGCCAGGATATACG-3') and CreR (5'-AATCGC CATCTTCCAGCAG-3').

Immunoblot analysis

Tissue samples and embryos were homogenized in ice-cold phosphate buffered saline (PBS) at pH 7.4, and protein lysates were prepared by sonicating cell pellets in lysis buffer containing 2.5 mM Tris–HCl (pH 7.4), 2% sodium dodecyl sulfate, 1%Triton X-100, 1 mM EDTA and Complete^{TM} protease inhibitor (Roche Molecular Biochemicals, Indianapolis, IN, USA). Protein lysates were fractionated by 7.5% SDS-PAGE and transferred onto nitrocellulose membranes. The membranes were blocked with 1% casein solution and incubated in blocking buffer at 4 °C overnight with rabbit anti-Atp7a antibody (1:4000 dilution) [6, 7], or rabbit anti-tubulin antibody (1:4000) (Sigma, St. Louis, MO, USA). Horseradish peroxidase conjugated goat anti-rabbit IgG (1:4000; Sigma) was used as a secondary antibody, and blots were developed using the SuperSignal West Pico Substrate according to the manufacturer's instructions (Pierce, Rockford, IL, USA).

Rotarod analyses

Mice underwent training over three consecutive days on an IITC Life Science Rotarod Treadmill (Woodland Hills, CA, USA) with an increasing ramp speed from 2.5 rpm to 25 rpm in 180 s. On the fourth day, latency to fall (or until the mouse clasped onto the rod and began rotating with it) was recorded three times per mouse with the longest duration used to generate mean scores for each age group and genotype.

Grip strength analyses

Grip strength was simultaneously measured across four paws using the Grip Strength Test apparatus (Bioseb, Paris, France). Resistance was measured in grams and normalized to body weight. Four tests were recorded for each mouse with the maximum value used to generate mean scores for each age group and genotype.

Gait analysis

Gait was assessed by using the Catwalk XT Gait Analysis system (Noldus Information Technology, Asheville, NC). Mice were allowed to freely ambulate along an illuminated glass plate within a confined corridor and footprints were recorded with a high-speed camera. Three compliant (time constrained) trials were analyzed per animal, averaged and the mean of the average calculated per genotype.

Thermal hyperalgesia

Thermal hyperalgesia was tested using a Hargreave's Plantar Test (UCSD, San Diego, CA) as previously described [8]. Thermal stimulus from a focused projection bulb was directed underneath a hind paw, and latency to remove or lick paw was recorded and converted to a corresponding temperature. In all cases, a maximum of 20 s was used to avoid injury. Four measurements were taken per hind paw and averaged.

Mechanical algesia

Mechanical algesia was measured with a Dynamic Plantar Aesthesiometer (DPA) model # 37450 (Ugo Basile, Italy). Mice were set on a wire-mesh platform and a metal filament was pushed against the hind paws with a linear ascending force (10 g/s) until a strong, immediate withdrawal occurred. Measurements were recorded in triplicate and averages were reported as paw withdrawal thresholds in grams.

Tissue preparation, immunofluorescence and muscle analysis

Anaesthetized mice were transcardially perfused with 4% paraformaldehyde. Tissues were removed, post-fixed for 16 hours in 4% paraformaldehyde at 4 °C. For immunofluorescence microscopy tissues were cryoprotected in 20% sucrose overnight, prior to sectioning on a cryostat at 25 μm thickness for gastrocnemius muscle, and 10 μm thickness for spinal cord. Prepared cryosections were incubated in ice-cold acetone for 5 min, washed several times with PBST and blocked for 2 hours in 1% casein solution in PBS. Sections were then incubated with rabbit anti-Atp7a antibody (1:3000) and SMI-32 antibody (1:1000) (Covance, Princeton, NJ), or SMI-31 antibody (1:500) (Covance, Princeton, NJ), and Alexa 594-conjugated α-bungarotoxin (1:2000) (Life Technologies, Carlsbad, CA) overnight at 4 °C washed three times with PBS and incubated for 1 hour at room temperature with appropriate secondary Alexa 488- or Alexa 594 antibodies (1:4000) (Life Technologies). Complete co-localization of α-bungarotoxin with neurofilament markers was considered muscular innervation, and α-bungarotoxin staining alone represents a denervated junction. A total of 100 neuromuscular junctions were analyzed per animal, with four animals analyzed per genotype. For tissue histology, postfixed tissues were cryopreserved in 20% sucrose overnight, embedded in paraffin and 4 μm sections were stained with hematoxylin and eosin. For motor neuron counts, lumbar spinal cords were cryopreserved and 10 μm cross-sections and every 12th section was stained with 1% Cresyl Violet over four sections from four different mice per genotype. Images were analyzed using ImageJ software to count motor neuron cell bodies larger than 100 μm^2. Cell counts were made within an area demarcated by a horizontal line drawn through the central canal and encompassing the ventral horn. For g-ratio counts, fixed sciatic nerves were dissected, and semi-thin sections (0.5–1 μm) were

stained with 1% toluidine blue. G-ratios were calculated using ImageJ software. Averages were calculated for 100 nerves per section, and three sections per mouse and three mice per genotype. For staining using copper sensor 3 (CS3), fixed spinal cord cryosections (10μm) were incubated with 4 μM CS3 for 10 minutes at room temperature, and washed three times in PBS before mounting and imaging [9, 10].

Enzyme assays

Haemoglobin concentrations were determined spectrophotometrically as metcyanohaemoglobin [11], and serum ceruloplasmin activity was measured by the oxidation of *O*-dianisidine as previously described [12].

Inductively coupled plasma mass spectrometry (ICP MS)

Lumbar spinal cords were dissolved in 70 % nitric acid overnight at room temperature and then at 75°C for 2 h. Metal levels were measured by inductively coupled plasma mass spectrometry (ICP-MS). The instrument (Agilent 7500cx coupled to a SC-DX4 autosampler from Elemental Scientific Inc) was operated in collision/reaction mode (He 3.5 ml/min, H2 1.5 ml/min) with 50ppb Ga as an internal standard. Values were acquired in triplicate for each sample and the results were normalized to tissue wet weight.

Statistical analyses

Analyses were performed using PRISM (GraphPad Software Inc.) to calculate Student's t-test, or two-way ANOVA with Bonferonni post-test. *P* values were considered to be significant when less than 0.05.

RESULTS

Motor neuron-specific deletion of *Atp7a*

To evaluate the requirement for ATP7A in the motor neuron, we used the well-characterized Hb9-Cre transgenic mice to selectively delete the *Atp7a* gene within the motor neurons [13]. The *Hb9* gene is expressed in spinal cord somatic and visceral motor neurons beginning at embryonic day 9.5 [13–15]. Hb9-Cre males were crossed with females that were heterozygous for the floxed *Atp7a* allele [6, 7]. The resulting male progeny that inherited both the floxed allele and the Cre transgene, hereafter called $Atp7a^{MN/Y}$ mice, were born at the expected Mendelian frequency, and at birth were indistinguishable from littermate controls. Immunoblot analysis revealed a marked reduction in the levels of ATP7A protein in lysates derived from the lumbar region of the spinal cord of $Atp7a^{MN/Y}$ mice at age P21 compared to age-matched wild type mice, but not in a range of other tissues including liver, muscle, kidney, spleen, and intestine (Figure 1A). In wild type mice, immunofluorescence analysis of cryosections derived from the lumbar region of the spinal cord revealed robust staining of the ATP7A protein in the perinuclear region of cells positive for the motor neuron neurofilament marker protein, SMI-32 (Figure 1B). In contrast, ATP7A was essentially undetectable with this method in SMI-32 positive motor neurons of the $Atp7a^{MN/Y}$ mice (Figure 1B).

No differences in copper concentration were observed in the lumbar region of the spinal cords of mutant and wild type animals at 2 months of age (Figure 1C). However, by 6- and 12 months of age, copper concentrations were significantly decreased in the lumbar spinal cords from the *Atp7a*$^{MN/Y}$ mice compared to wild type animals (Figure 1C). Given the role of ATP7A in copper export, the finding that copper concentrations were decreased in spinal cords of aged *Atp7a*$^{MN/Y}$ mice was unexpected. Therefore, additional studies were undertaken to detect copper in fixed spinal sections of 4- and 8-month old mice using the fluorescent copper sensor, CS3 [9, 10]. Although CS3 produced significant general staining throughout the spinal sections, the motor neuron cell bodies of 8-month old *Atp7a*$^{MN/Y}$ mice exhibited an intense perinuclear staining that was absent in WT mice, consistent with hyperaccumulation of copper (Figure 1D). Total iron concentration in the lumbar spinal cord did not differ between WT and *Atp7a*$^{MN/Y}$ mice at any age tested (Supplemental Figure 1A). Parameters of systemic copper status were found to be normal in the *Atp7a*$^{MN/Y}$ mice including total copper concentrations in the liver and brain, serum ceruloplasmin activity and blood haemoglobin (Supplemental Figure 1B-E). Iron concentrations were also normal in the liver and brain of the *Atp7a*$^{MN/Y}$ mice (Supplemental Figure 1F and 1G). Taken together, these data suggest that deletion of ATP7A in the motor neuron results in an age-dependent increase in copper content of the motor neuron, which is accompanied by an overall reduction in copper concentration in the spinal cord.

Atp7a$^{MN/Y}$ *mice* exhibit progressive muscle atrophy

The size and total body weight were identical in *Atp7a*$^{MN/Y}$ mice and age-matched control animals over the course of one year (Figure 2A). However by 12 months of age the *Atp7a*$^{MN/Y}$ mice showed a decrease in muscle mass as determined by the weight of the gastrocnemius muscle (Figure 2B). This decrease was not apparent in these animals at 6 months of age, suggesting that muscle loss was a progressive late-onset phenotype. In contrast, gonadal fat content was elevated in the *Atp7a*$^{MN/Y}$ mice at 12 months of age (Figure 2C), suggesting that these tissue specific changes account for the normal body weight in these animals. While no differences in muscle histology were observed between *Atp7a*$^{MN/Y}$ mice and control animals at 6 months of age, by 12 months the gastrocnemius muscle from the *Atp7a*$^{MN/Y}$ mice exhibited a loss of muscle bundles and the presence of inclusion bodies (Figure 2D and 2E).

Atp7a$^{MN/Y}$ *mice* exhibit progressive degeneration of motor function without sensory loss

An initial test of motor function was performed by assessing the splaying hind limb posture upon tail suspension. Whereas this response was normal in the *Atp7a*$^{MN/Y}$ mice at 2 months of age, by 6 months of age these animals exhibited abnormal clasping of the legs and digits upon tail suspension (Figure 3A). Grip strength, measured simultaneously across all four limbs, was found to be significantly reduced in the *Atp7a*$^{MN/Y}$ mice by 6 months of age compared to wild type mice (Figure 3B). Similarly, rotarod analyses revealed a significantly shorter latency to fall for the *Atp7a*$^{MN/Y}$ mice relative to controls by 6 months (Figure 3C). Analysis of freely ambulating mice demonstrated that while gaiting parameters were normal in *Atp7a*$^{MN/Y}$ mice at 2- and 4 months of age, by 8 months of age, the *Atp7a*$^{MN/Y}$ mice exhibited significant reductions in the percentage of overlapping footfalls (Figure 4A and 4B). By 6 months of age the frequency of diagonal contacts in freely ambulating *Atp7a*$^{MN/Y}$

mice was significantly lower than wild type animals, and accompanied by compensatory increases in triagonal contacts (Figure 4C and 4D). Consistent with the concept that these defects are specific to the motor neuron, no differences were detected between *Atp7a*$^{MN/Y}$ and wild type mice at 6 and 12 months of age in response to either thermal or mechanical stimulation (Supplemental Figure 2).

Atp7a$^{MN/Y}$ *mice* exhibit loss of motor neuron cell bodies and denervation of the neuromuscular junctions

To examine the neuromuscular pathology associated with these phenotypes, spinal cords were sectioned and stained with Cresyl Violet, and the motor neuron cell bodies in the ventral horn were enumerated. As shown in Figure 5, by 12 months of age the *Atp7a*$^{MN/Y}$ mice possessed fewer motor neurons compared to age-matched wild type mice (Figure 5A) Representative images from sections derived from 12-month-old mice are shown in Supplementary Figure 3A. To examine the role of demyelination in the observed phenotypes, semi-thin sciatic nerve sections were prepared and bright field microscopy was used to calculate the motor neuron g-ratios, defined as the ratio of the inner axonal diameter to the outer total diameter. No differences in g-ratio (or axonal numbers) were found between wild type and *Atp7a*$^{MN/Y}$ mice at 6, 8 and 12 months of age (Figure 5B), indicating that motor dysfunction at these ages is not attributable to alterations in axonal diameter or myelin thickness. Representative images from these sections derived from 12-month-old mice are shown in Supplementary Figure 3B. In contrast, symptomatic *Atp7a*$^{MN/Y}$ mice exhibited a significant decrease in the percentage of innervated neuromuscular junctions relative to wild type mice at 6 and 8 months of age, and this was further decreased by 12 months (Figure 5C and Supplementary Figure 3C). Taken together, these data support the concept that loss-of-function of *Atp7a* in the motor neuron results in an age dependent motor neuropathy resulting from aberrant copper homeostasis.

Discussion

The results of this study demonstrate that loss-of-function of ATP7A within the lower motor neurons of mice results in the progressive onset of gait defects, loss of limb strength, muscle wasting, and histopathological changes that collectively phenocopy human SMAX3 (Figure 6) [4]. The observation that denervation of the neuromuscular junctions in *Atp7a*$^{MN/Y}$ mice precedes the loss of motor neuron cell bodies is characteristic of a “dying back” phenomenon in which degeneration begins in the distal portions of axons and retreats towards the motor neuron cell body (Figure 6). In addition, the normal g-ratio in affected animals indicates a lack of myelin pathology, which is consistent with the finding of normal conduction velocities in affected patients. The delayed onset of these neuromuscular phenotypes recapitulates the disease progression observed in patients, which typically appears in the third decade of life [3]. The reason for the accompanying increase in gonadal fat is not clear, however, as this phenotype was restricted to symptomatic animals it may reflect reduced energy expenditure as the motor deficits became more pronounced. Taken together, the findings indicate that despite any evidence of systemic abnormalities in copper homeostasis, these neurologic symptoms are associated with motor neuron accumulation of copper and progressive decrease in the copper content of the lumbar spine. It is currently

unclear why loss of ATP7A in the motor neuron resulted in lower spinal copper levels. It is possible that chronic copper overload in the motor neuron may trigger regulatory mechanisms that limit copper levels in the spinal cord. Alternatively, these changes in spinal copper may arise from motor neuron loss or other pathological sequelae. Further exploration of localized copper levels within the motor neuron and surrounding cells using more quantitative approaches such as X-ray fluorescence microscopy will shed light on this phenomenon.

The phenotypic similarity between *Atp7a*$^{MN/Y}$ mice with human SMAX3 suggests that the two unique *ATP7A* gene missense mutations identified in SMAX3 patients cause motor neuropathy via a loss of function mechanism. Previous studies have shown that the missense mutations identified in affected patients reduce copper transport function by approximately 20–24%, however the mechanism by which the motor neuron is specifically affected is unknown [4]. While such a reduction in ATP7A activity would appear to have little impact on copper transport across the intestinal epithelium, as evidenced by the absence of systemic copper deficiency in these patients [4], even a partial reduction in ATP7A activity may preferentially disrupt copper homeostasis in specific tissues, that over time impacts a vulnerability in the motor neuron. Glutamate is known to stimulate ATP7A-dependent release of copper from hippocampal neurons as a feedback mechanism to suppress calcium influx and downstream signaling [16, 17]. ATP7A may serve in a similar capacity to regulate cholinergic or glutamatergic signaling in motor neurons [18–20]. Alternatively, it is possible that these two mutations result in an impaired function of ATP7A only within the motor neuron as a result of unique protein interactions that inactivate ATP7A [5]. In either case, the data reported here clearly indicate that the loss of ATP7A function is an essential component of disease pathogenesis.

Distal hereditary motor neuropathies comprise a clinically heterogeneous group of disorders with diverse genetic etiologies (4), and despite recent progress in their genetic characterization, the underlying disease mechanisms remain obscure. The striking phenotypic similarity between *Atp7a*$^{MN/Y}$ mice and human SMAX3 patients suggests that this disorder is caused by partial loss of ATP7A activity that preferential impacts the motor neuron. The *Atp7a*$^{MN/Y}$ mice will provide a useful animal model to elucidate the specific requirement for copper in this form of distal hereditary motor neuropathy, as well as the effect of high and low dietary copper intake on disease pathogenesis, which may allow for the development of novel therapeutic approaches in affected patients.

Supplementary Material

Refer to Web version on PubMed Central for supplementary material.

ACKNOWLEDGMENTS

We thank members of our laboratories for helpful comments throughout this project. We thank Chris Chang (U.C. Berkeley) for kindly providing the CS3 reagent. This work was supported by grants DK093386 (MJP) and DK079209 (JL) from the National Institutes of Health, and a grant from the University of Missouri Spinal Cord Injury Research Program (MJP).

REFERENCES

1. Petris MJ, Mercer JF, Culvenor JG, et al. Ligand-regulated transport of the Menkes copper P-type ATPase efflux pump from the Golgi apparatus to the plasma membrane: a novel mechanism of regulated trafficking. The EMBO journal. 1996; 15:6084–6095. [PubMed: 8947031]
2. Kaler SG, Holmes CS, Goldstein DS, et al. Neonatal diagnosis and treatment of Menkes disease. The New England journal of medicine. 2008; 358:605–614. [PubMed: 18256395]
3. Kaler SG. ATP7A-related copper transport diseases-emerging concepts and future trends. Nature reviews Neurology. 2011; 7:15–29.
4. Kennerson ML, Nicholson GA, Kaler SG, et al. Missense mutations in the copper transporter gene ATP7A cause X-linked distal hereditary motor neuropathy. American journal of human genetics. 2010; 86:343–352. [PubMed: 20170900]
5. Yi L, Donsante A, Kennerson ML, et al. Altered intracellular localization and valosin-containing protein (p97 VCP) interaction underlie ATP7A-related distal motor neuropathy. Human molecular genetics. 2012; 21:1794–1807. [PubMed: 22210628]
6. Wang Y, Zhu S, Hodgkinson V, et al. Maternofetal and neonatal copper requirements revealed by enterocyte-specific deletion of the Menkes disease protein. American journal of physiology Gastrointestinal and liver physiology. 2012; 303:G1236–G1244. [PubMed: 23064757]
7. Wang Y, Zhu S, Weisman GA, et al. Conditional knockout of the Menkes disease copper transporter demonstrates its critical role in embryogenesis. PloS one. 2012; 7:e43039. [PubMed: 22900086]
8. Dirig DM, Salami A, Rathbun ML, et al. Characterization of variables defining hindpaw withdrawal latency evoked by radiant thermal stimuli. Journal of neuroscience methods. 1997; 76:183–191. [PubMed: 9350970]
9. Dodani SC, Domaille DW, Nam CI, et al. Calcium-dependent copper redistributions in neuronal cells revealed by a fluorescent copper sensor and X-ray fluorescence microscopy. Proceedings of the National Academy of Sciences of the United States of America. 2011; 108:5980–5985. [PubMed: 21444780]
10. Hong-Hermesdorf A, Miethke M, Gallaher SD, et al. Subcellular metal imaging identifies dynamic sites of Cu accumulation in Chlamydomonas. Nature chemical biology. 2014; 10:1034–1042.
11. Prohaska JR. Changes in Cu,Zn-superoxide dismutase, cytochrome c oxidase, glutathione peroxidase and glutathione transferase activities in copper-deficient mice and rats. The Journal of nutrition. 1991; 121:355–363. [PubMed: 1848285]
12. Prohaska JR. Changes in tissue growth, concentrations of copper, iron, cytochrome oxidase and superoxide dismutase subsequent to dietary or genetic copper deficiency in mice. The Journal of nutrition. 1983; 113:2048–2058. [PubMed: 6312000]
13. Arber S, Han B, Mendelsohn M, et al. Requirement for the homeobox gene Hb9 in the consolidation of motor neuron identity. Neuron. 1999; 23:659–674. [PubMed: 10482234]
14. Yang X, Arber S, William C, et al. Patterning of muscle acetylcholine receptor gene expression in the absence of motor innervation. Neuron. 2001; 30:399–410. [PubMed: 11395002]
15. Alaynick WA, Jessell TM, Pfaff SL. SnapShot: spinal cord development. Cell. 2011; 146:178–178. e171. [PubMed: 21729788]
16. Schlief ML, Gitlin JD. Copper homeostasis in the CNS: a novel link between the NMDA receptor and copper homeostasis in the hippocampus. Molecular neurobiology. 2006; 33:81–90. [PubMed: 16603790]
17. Schlief ML, Craig AM, Gitlin JD. NMDA receptor activation mediates copper homeostasis in hippocampal neurons. The Journal of neuroscience : the official journal of the Society for Neuroscience. 2005; 25:239–246. [PubMed: 15634787]
18. Nishimaru H, Restrepo CE, Ryge J, et al. Mammalian motor neurons corelease glutamate and acetylcholine at central synapses. Proceedings of the National Academy of Sciences of the United States of America. 2005; 102:5245–5249. [PubMed: 15781854]
19. Lee Y, Morrison BM, Li Y, et al. Oligodendroglia metabolically support axons and contribute to neurodegeneration. Nature. 2012; 487:443–448. [PubMed: 22801498]
20. Micu I, Jiang Q, Coderre E, et al. NMDA receptors mediate calcium accumulation in myelin during chemical ischaemia. Nature. 2006; 439:988–992. [PubMed: 16372019]

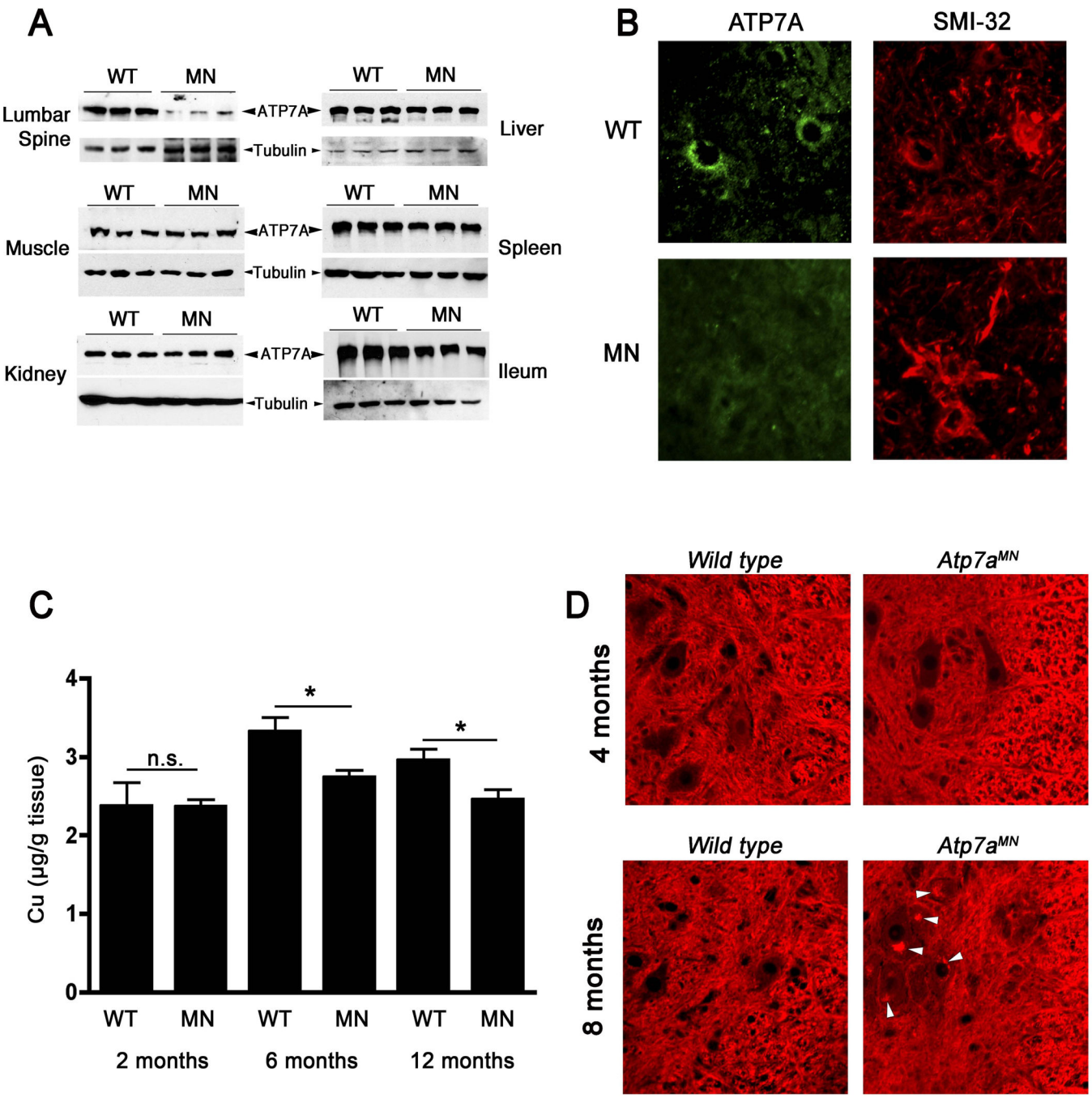

Figure 1. Motor neuron-specific knockout of Atp7a

(A) Tissue-specificity of *Atp7a* knockout. Immunoblot analysis reveals a lack of ATP7A protein in lumbar spinal cord lysates derived from the $Atp7a^{MN/Y}$ mice (MN) relative to wild type littermate controls (WT) at age P21. Tubulin is detected as a loading control. Other tissues derived from the $Atp7a^{MN/Y}$ mice including liver, muscle, spleen, kidney, and intestine show no reduction in ATP7A protein. (B) Immunofluorescence microscopy of lumbar spinal sections was used to detect ATP7A protein (green) within SMI-32 positive motor neuron cell bodies (red). Note the lack of ATP7A in SMI-32 positive motor neurons

of *Atp7a*$^{MN/Y}$ mice. (C) Lumbar spine copper concentrations were decreased at both 6- and 12- months of age in *Atp7a*$^{MN/Y}$ mice as compared to control mice (mean +/− S.E.M., n = 4 mice per genotype; Student's t-test, *$p<0.05$). (D) Copper accumulation within the motor neurons of aged *Atp7a*$^{MN/Y}$ mice. Lumbar spinal sections from 4- and 8-month-old mice were stained with the copper sensor CS3. Note the increased CS3 staining in localized perinuclear compartments within motor neuron cell bodies of MN mice at 8 months of age compared to WT controls (arrowheads), but no such difference was apparent at 4 months.

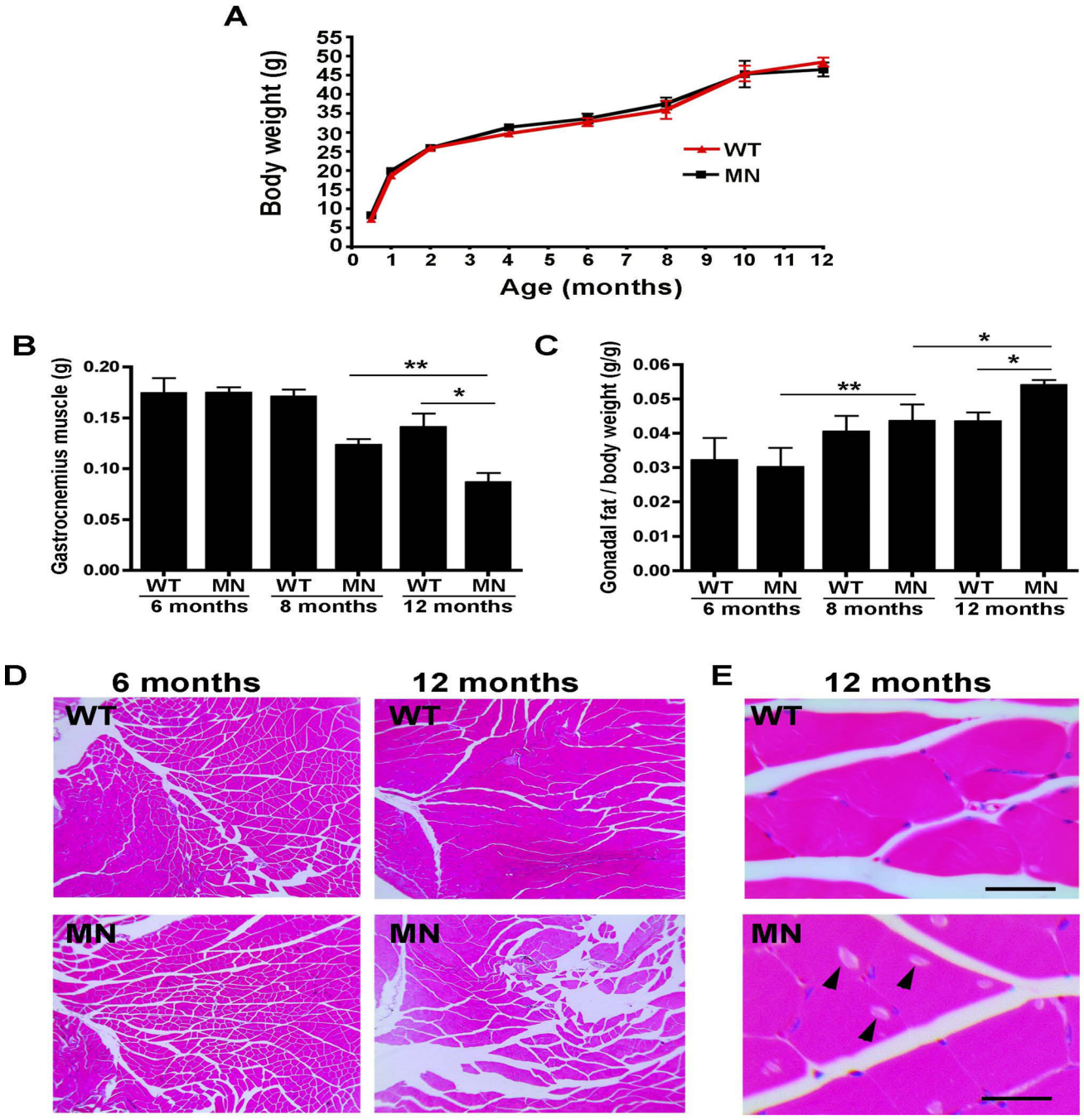

Figure 2. *Atp7a*$^{MN/Y}$ mice exhibit progressive muscle atrophy

(A). Growth analysis of *Atp7a*$^{MN/Y}$ mice. No difference in total weight was found between *Atp7a*$^{MN/Y}$ mice (MN) and WT controls over a one-year time course (n=12 per genotype; mean +/− S.E.M.). (B) Gastrocnemius muscle weight of *Atp7a*$^{MN/Y}$ mice was decreased in comparison to WT controls at 12 months of age, but not at 6- or 8 months (n=5 per genotype; mean +/− S.E.M., Student's t-test,*p<0.05, **p<0.01). (C) Gonadal fat pad weight as a proportion of body weight was increased in *Atp7a*$^{MN/Y}$ mice at 12 months of age, but not at 6- or 8 months (n=5 per genotype; mean +/− S.E.M., Student's t-test,

*p<0.05, **p<0.01). (D) Age-dependent muscle pathology in the *Atp7a*$^{MN/Y}$ mice. Haemotoxylin and eosin stain of gastrocnemius muscle shows increased muscle clearance in *Atp7a*$^{MN/Y}$ mice compared to WT mice at 12 months of age, but not at 6 months of age. (E) A 60x magnification reveals inclusion bodies (arrowheads) in 12-month-old *Atp7a*$^{MN/Y}$ mice, but not in control mice. Scale bar, 50μm.

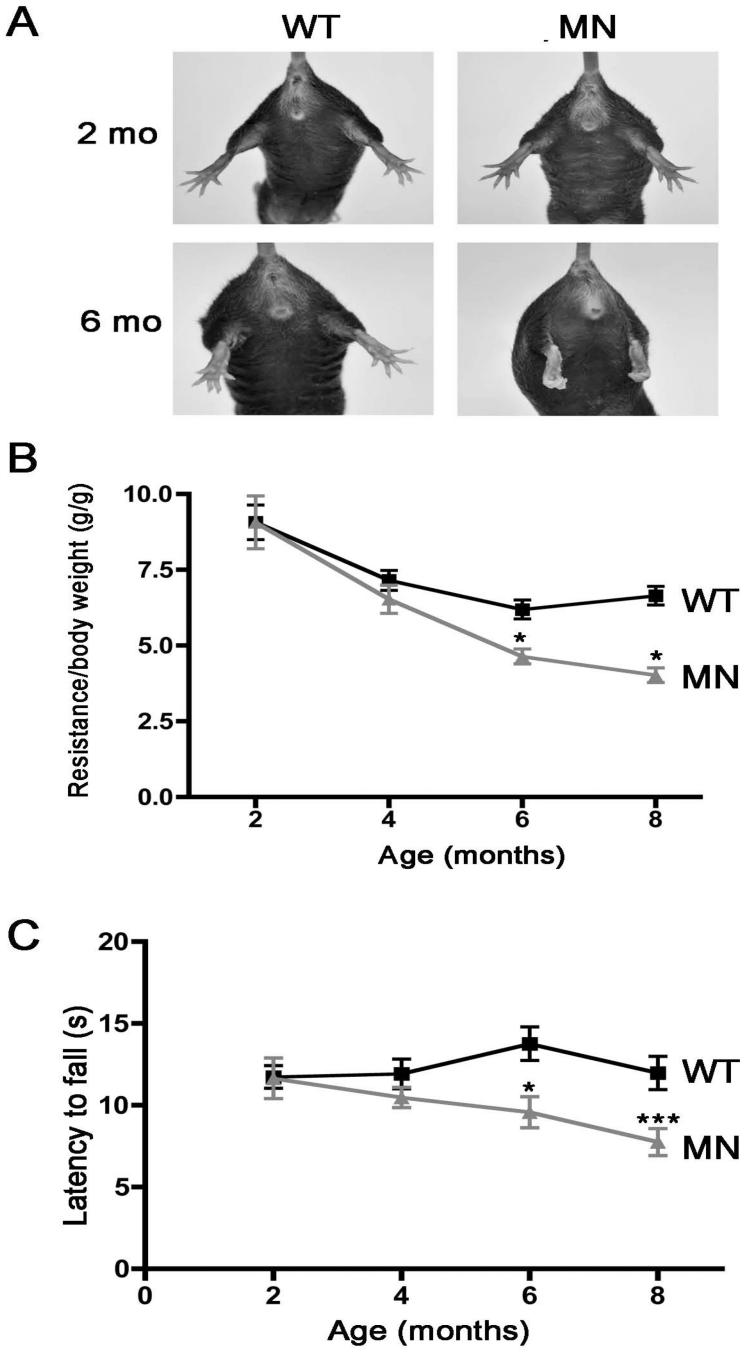

Figure 3. *Atp7a*$^{MN/Y}$ mice exhibit progressive motor abnormalities

(A) Abnormal hind limb posture in *Atp7a*$^{MN/Y}$ mice upon tail suspension. The reflexive splaying of the hind limbs and digits in response to elevation by the tail was absent in the *Atp7a*$^{MN/Y}$ mice by 6 months of age, but not at 2 months. (B) Grip strength across all four limbs was decreased in the *Atp7a*$^{MN/Y}$ mice compared to WT controls between 4- and 6 months of age, with no significant differences at 2 months (n=6 per genotype; mean +/− S.E.M., 2 way ANOVA with post Bonferonni, *p<0.05). (C) Rotarod analysis shows that latency to fall was decreased in *Atp7a*$^{MN/Y}$ mice by 6 months of age in comparison to WT

controls. No significant differences were detected in animals at 2- and 4 months of age (n=10 per genotype; mean +/− S.E.M., 2 way ANOVA with post Bonferonni, *p<0.05, ***p<0.001).

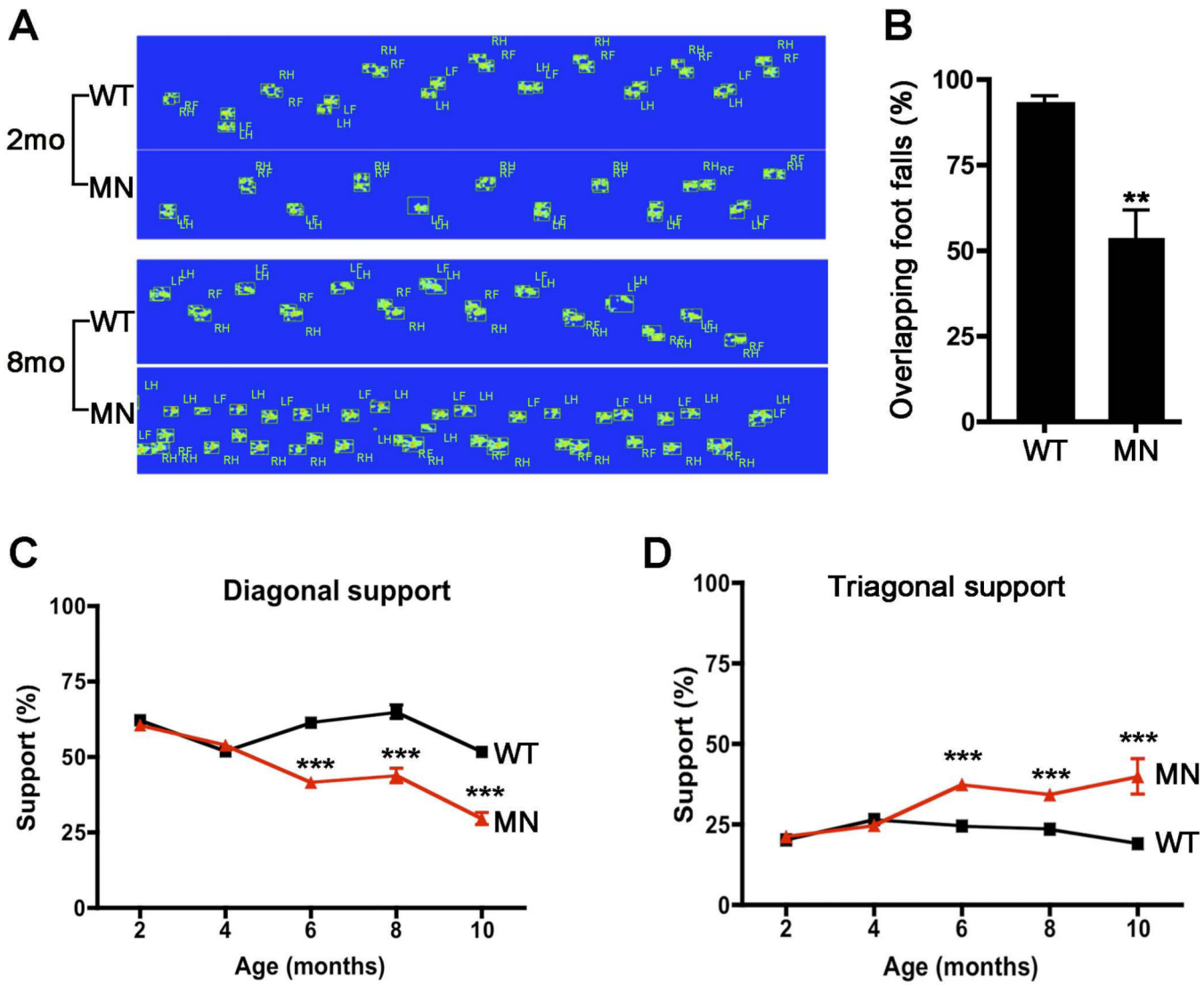

Figure 4. Age-dependent gait abnormalities in the *Atp7a*$^{MN/Y}$ mice

(A) Representative footfall tracings of freely ambulating wild type and *Atp7a*$^{MN/Y}$ mice at 2- and 8- months of age revealing a high degree of non-overlapping footfalls in the 8 month-old *Atp7a*$^{MN/Y}$ mice. (LF, left front; LH, left hind; RF, right front; RH, right hind). (B) Quantification of overlapping footfalls for wild type and *Atp7a*$^{MN/Y}$ mice at 8 months of age (n = 6 per genotype; mean +/− S.E.M., Student's t-test, **p<0.01). (C and D) Analysis of simultaneous diagonal- and triagonal support in ambulating mice. By 6 months of age *Atp7a*$^{MN/Y}$ mice exhibited a decrease in diagonal support (simultaneous diagonal contacts) and a concomitant increase in triagonal supports (n=15 per genotype; mean +/− S.E.M., 2-way ANOVA with post Bonferonni, ***p<0.001).

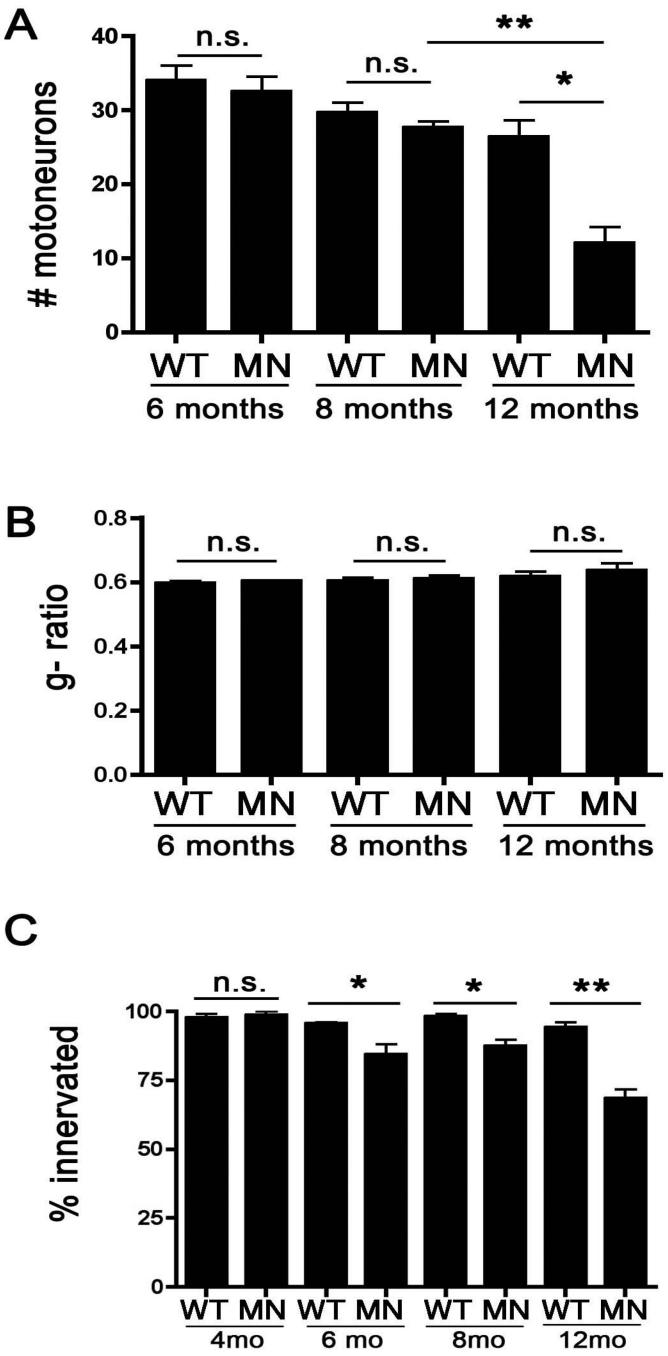

Figure 5. *Atp7a*$^{MN/Y}$ mice exhibit age-dependent loss of motor neuron cell bodies and denervation of the neuromuscular junction

(A) Motor neuron counts in the ventral horn of Cresyl violet-stained lumbar spinal sections. *Atp7a*$^{MN/Y}$ mice exhibited fewer motor neurons at 12 months of age compared to age-matched control mice, however, no significant differences were found in younger animals (mean +/− S.E.M., Student's t-test, n = 3 or 4 mice per genotype; *p<0.05, **p<0.01). (B) Quantification of the motor neuron g-ratio in wild type and *Atp7a*$^{MN/Y}$ mice. The average ratio of the inner axonal diameter to the outer total diameter was calculated from semi-thin

sciatic nerve sections stained with toluidine blue. No differences in g-ratios were found between wild type and *Atp7a*$^{MN/Y}$ mice at all ages tested (n = 3 mice per genotype, 300 axons per animal). (C) Neuromuscular junction innervation. The gastrocnemius muscle was sectioned and immunofluorescence analysis of innervation scored by determining overlapping signal of SMI-31 (nerve) with α-bungarotoxin (muscle junction). *Atp7a*$^{MN/Y}$ mice exhibited a decrease in the percentage of innervated junctions compared to control mice at 6-, 8- and 12 months of age, but not at 4 months of age (mean +/− S.E.M., n = 3 or 4 mice per genotype, mean of 100 neuromuscular junctions per mouse; Student's t-test, *p<0.05; **p<0.01).

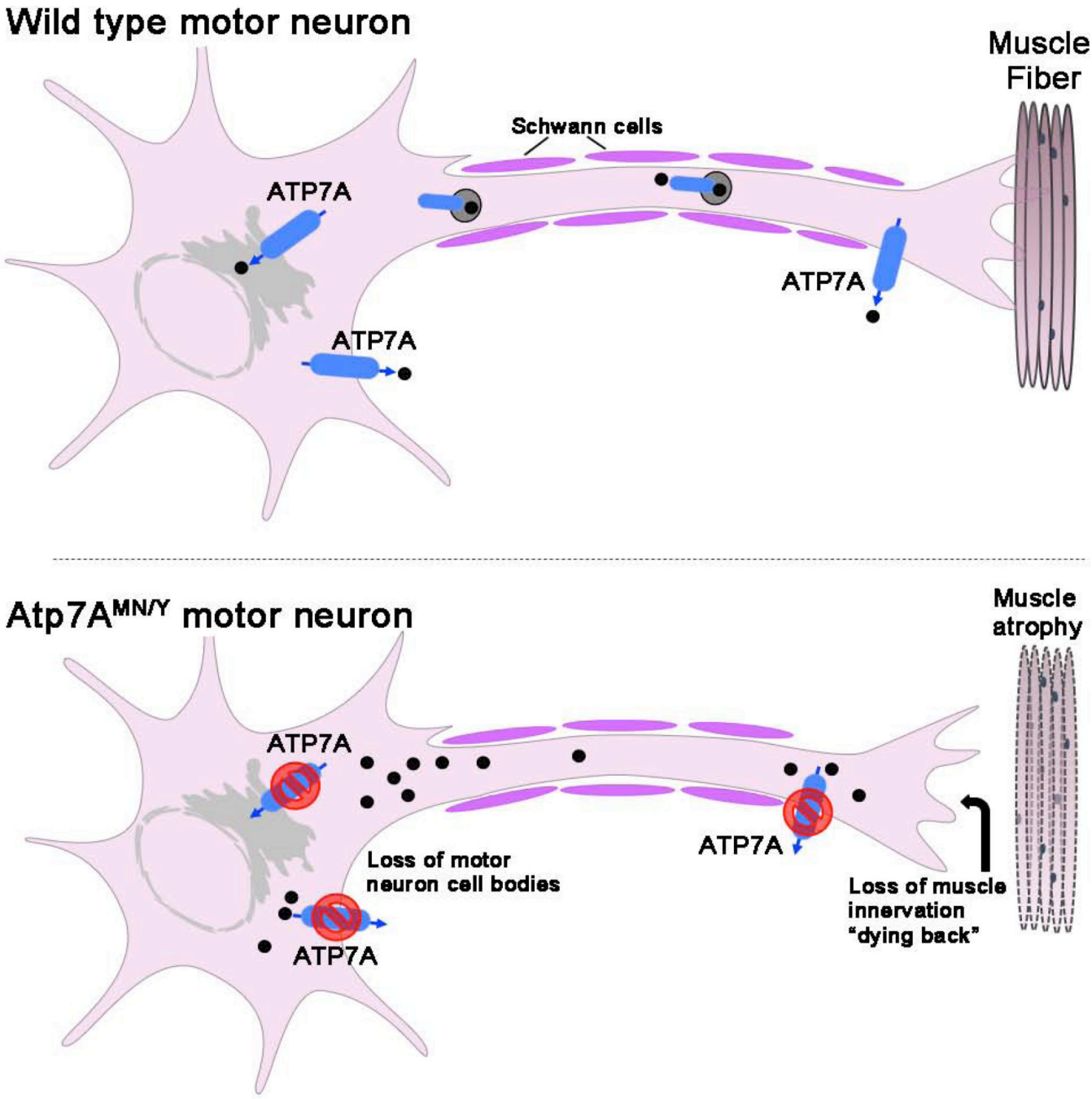

Figure 6. Schematic model for SMAX3-like pathology in *Atp7a*$^{MN/Y}$ mice

Predicted roles of ATP7A are shown including copper transport into the secretory pathway to metallate copper dependent enzymes and copper export. The lower panel depicts the consequences of motor neuron loss of ATP7A function exhibited by *Atp7a*$^{MN/Y}$ mice including copper hyperaccumulation, muscle atrophy, loss of muscle innervation (dying back) and loss of motor neuron cell bodies. The resemblance of these phenotypes with human SMAX3 suggests a model in which 'dying back' axonopathy and muscle atrophy in

human patients is caused by partial loss of ATP7A function caused by T994I and P1386S mutations that specifically impact motor neuron function.